Coupling of DNA Circuit and Templated Reactions for Quadratic Amplification and Release of Functional Molecules

Kim, Kitae; Angerani, Simona; Chang, Dalu; Winssinger, Nicolas

How to cite

KIM, Kitae et al. Coupling of DNA Circuit and Templated Reactions for Quadratic Amplification and Release of Functional Molecules. In: Journal of the American Chemical Society, 2019, vol. 141, n° 41, p. 16288–16295. doi: 10.1021/jacs.9b05688

This publication URL: https://archive-ouverte.unige.ch//unige:124481
Publication DOI: 10.1021/jacs.9b05688

Coupling of DNA Circuit and Templated Reactions for Quadratic Amplification and Release of Functional Molecules

Ki Tae Kim, Simona Angerani, Dalu Chang and Nicolas Winssinger*

Department of Organic Chemistry, NCCR Chemical Biology, Faculty of Science, University of Geneva, 30 quai Ernest Ansermet, 1211 Geneva, Switzerland.

ABSTRACT: DNA-based circuitry empowers logic gated operations and amplifications but are restricted to a nucleic acid output. Templated reactions enable the translation of a nucleic acid cues into diverse small molecule outputs but are more limited in their amplification. Herein, we demonstrate the coupling of a DNA circuit to templated reactions in order to achieve high levels of amplification in the output of small molecules, in response to a nucleic acid input. We demonstrate that the coupling of the DNA circuit to templated reactions allow for the detection of fM concentration of analyte and can respond with the release of a cytotoxic drug.

INTRODUCTION

The programmability and fidelity of hybridization makes DNA an attractive platform to design networks and assemblies with emergent properties or functions. Developments in DNA nanotechnologies have transformed our thinking about the applications of nucleic acids.[1-2] Like supramolecular chemistry,[3] DNA nanotechnology is leveraged on reversible interactions that exchange, error correct and respond. Exchanges between strands can be programmed through toehold (a single strand overhang) displacements with controlled kinetics.[4-5] Strand displacement mechanisms have been used to engineer networks capable of solving mathematical operations and circuits capable of amplification or molecular motion.[6-15] In parallel, DNA-templated reactions have also been shown to be a powerful strategy to translate a nucleic acid cue into a chemical reaction.[16-17] Whereas the output of strand-displacement networks are inherently oligonucleotides,[18] templated reactions can be used to uncage or synthesize functional molecules. It has been shown that strand displacement and templated reactions can be coupled to achieve logic-gated chemical transformation however,[13, 19] only a fluorescent output has been demonstrated thus far and templated reactions have not been coupled to DNA-based circuits for amplification. This would be particularly relevant for amplifications in which only low levels of inputs are available and insufficient to generate critical threshold of output. For instance, circulating microRNA are emerging as powerful biomarkers but are typically present in sub-nanomolar concentrations[20-21] and other noncoding RNAs continue to be identified.[22-23] While templated reactions are capable of signal amplification through template turn-over, few examples surpass 100-fold amplification, and this level of amplification requires long reaction times. Recently, several strategies have been reported in attempts to maximize amplifications in templated reactions, including designs that maximize template turn-over[24] and reaction cascades.[25] Herein, we report the use of a DNA circuit that respond to an oligonucleotide input with the formation and amplification of a competent catalyst for templated reactions (Figure 1).

The DNA circuit is designed such that the input is catalytic and thus amplifies the formation of the product, which in turns templates a reaction capable of turn-over (second amplification). The combined cycles of the DNA-circuit with templated reactions result in quadratic amplification.

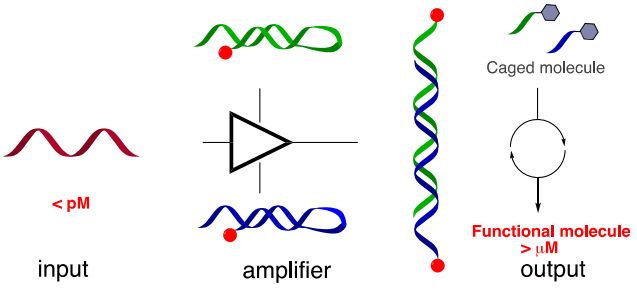

Figure 1. Schematic overview of DNA-fueled amplifier circuit coupled to templated reaction

RESULT AND DISCUSSION

We hypothesized that templated reactions operating on the products of a DNA amplification circuit would deliver exponential amplifications that surpass the performance of regular templated reactions (Figure 2). A prominent motif in the products of DNA amplification circuits is a sticky end, an unpaired short oligonucleotide at the end of a duplex. We envisioned that this short stretch of DNA would afford sites for templated reactions. The amplification circuit is based on two metastable hairpins functionalized with a ruthenium complex for templated photocatalysis. Since the sequence for templated reaction is part of the double-stranded stem region of the hairpin, it is not available for templated reaction.[26] An oligonucleotide trigger (initiator: **I**) opens the first hairpin by toehold displacement resulting in a duplex with a long single stand overhang. This product hybridizes to the second hairpin which in turns displaces the initiator.

The dsDNA product now has two hybridization sites open for templated reactions and the initiator turns over in further cycles of dsDNA formation. A central point to this double amplification is that the templated reactions make

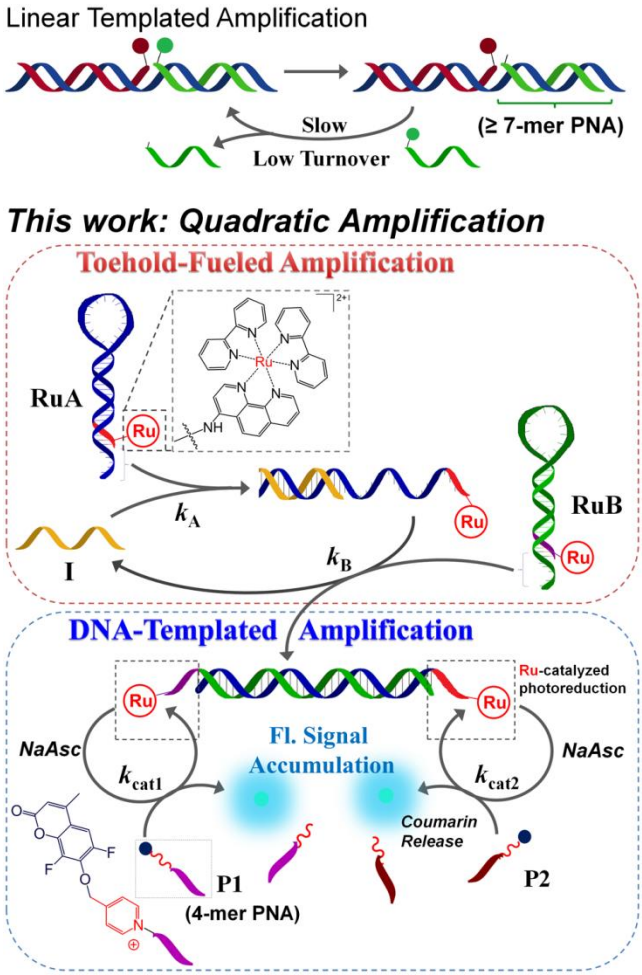

Figure 2. Schematic representation of linear templated amplification (top) and exponential amplification used designed in the present work (bottom).

use of a catalytic transformation such that each dsDNA formed can convert multiple substrates. The ruthenium photocatalysis is well suited for this purpose as it is capable of high turn-overs in photocatalyzed reductive reactions and has been shown to operate in complex biological environments.[27-29] The ground-state stability of the catalyst coupled to its excited state reactivity is key to its bioorthogonal chemistry.[30] Upon photoexcitation with 450 nm light and intersystem crossing, the Ru(II)* reacts with a stoichiometric reducing agent (NaAsc or NADPH in a biological environment) to afford a Ru(I) complex, a powerful single electron transfer (SET) reductant. The pyridinium linker is an excellent acceptor in a SET reaction leading to elimination of the coumarin and the pyridinium with a reduced benzylic position. While these reactions are very fast, the minimal length of the sticky end necessary for the templated reactions was unclear at the onset of this work. Prior analysis of the rate of templated reactions using PNA probes showed an optimal tradeoff between affinity (K_M) and turnover at 5-mer; reactions on shorter sequences were limited by the weak affinity (k_{off} too fast) while longer sequences were limited by product dissociation (k_{off} too slow).[26]

We began our study by optimizing the hairpin sequence for the DNA circuit, using an architecture inspired by a previous example of DNA fuel system.[8] We designed the sequence to respond to miR-21 and use the corresponding DNA sequence as initiator (**I**, miR-21-5p DNA). The length of stem and loop parts of two hairpins were adjusted to have the best meta-stability in the absence of **I** without compromising the rate of the DNA circuit. Several pairs of hairpins were tested, and **A** + **B** hairpin pair having 7-mer overhang, 14-mer stem, and 9-mer loop was found to perform best (Figure 3A, see Figure S1 for different combinations tested). At 37°C, hairpin **A** and **B** (50 nM) yielded >95% conversion into **AB** duplex within 1 h in the presence of 0.125 eq of **I**, without any leakage products (uninitiated duplex formation, Figure 3B). Based on this successful design of DNA hairpins, a ruthenium photocatalyst ($Ru(bpy)_2phen$) was introduced into 5′ end of each **A** and **B** hairpin to produce **RuA** and **RuB** for templated reactions. Likewise, the formation of the **RuAB** duplex in the presence of **I** was monitored by the gel electrophoresis. While the behavior of the **RuA** and **RuB** circuit paralleled the performance of unmodified hairpins (**A**+**B**), Ru-modified hairpins exhibited slower kinetics (Figure 3C, less than 50 % conversion with 0.125 eq of **I**), presumably due to additional stabilization of hairpins by the electrostatic interaction between DNA and the cationic ruthenium conjugate. To counter this effect and restore the rate of the DNA circuit, we investigate the addition of magnesium chloride in the buffer and found that indeed, there was a positive correlation between the circuit rate and $MgCl_2$ (Figure 3C, see Figure S2 for titration); 8-12 mM magnesium was sufficient to restore the rate of the circuit. This concentration is in line with biological conditions considering cell culture buffers often contain up to 10 mM of magnesium[31-32] and seawater contain ~50 mM.[33] Importantly, the magnesium had no impact on the leakage of the DNA circuit (Figure 3C, lane 7 from left).

To quantify the kinetics of the DNA circuit, fluorescence quenching experiments were carried out using dabsyl-conjugated hairpin (**Dab-A**) and fluorescein-conjugated initiator (**FAM-I**). The hybridization of **FAM-I** and **Dab-A** results in the quenching of the fluorescein signal by dabcyl while introduction of **RuB** leads to release of **FAM-I** from **Dab-A** and recovery of fluorescence signal. The reactions were approximated as pseudo-1st-order when one of the reactants is in large excess (e.g., [**Dab-A**] >> [**FAM-I**]). We measured a half-life of each step, finding the rate constants k_A and k_B of 2.3×10^6 and 5.1×10^5 M^{-1} s^{-1} at 37 °C and 1.6×10^6 and 3.0×10^5 M^{-1} s^{-1} at 25 °C, respectively (Figure 3D, see Figure S3 for expanded analysis of pseudo 1st order analysis).

The circuit works both at room temperature or physiological temperature and, as expected, is slightly faster in the latter case (~2-times). The kinetic was also measured using a second order rate constant analysis by the addition of stochiometric amount of **Dab-A** to **FAM-I** followed by stochiometric amount of **RuB** (Figure 3E). Interestingly, comparison of rates for **B** *vs* **RuB** in the second step of the circuit (**I:A** + **B** → **A:B** + **I**) showed that the cationic

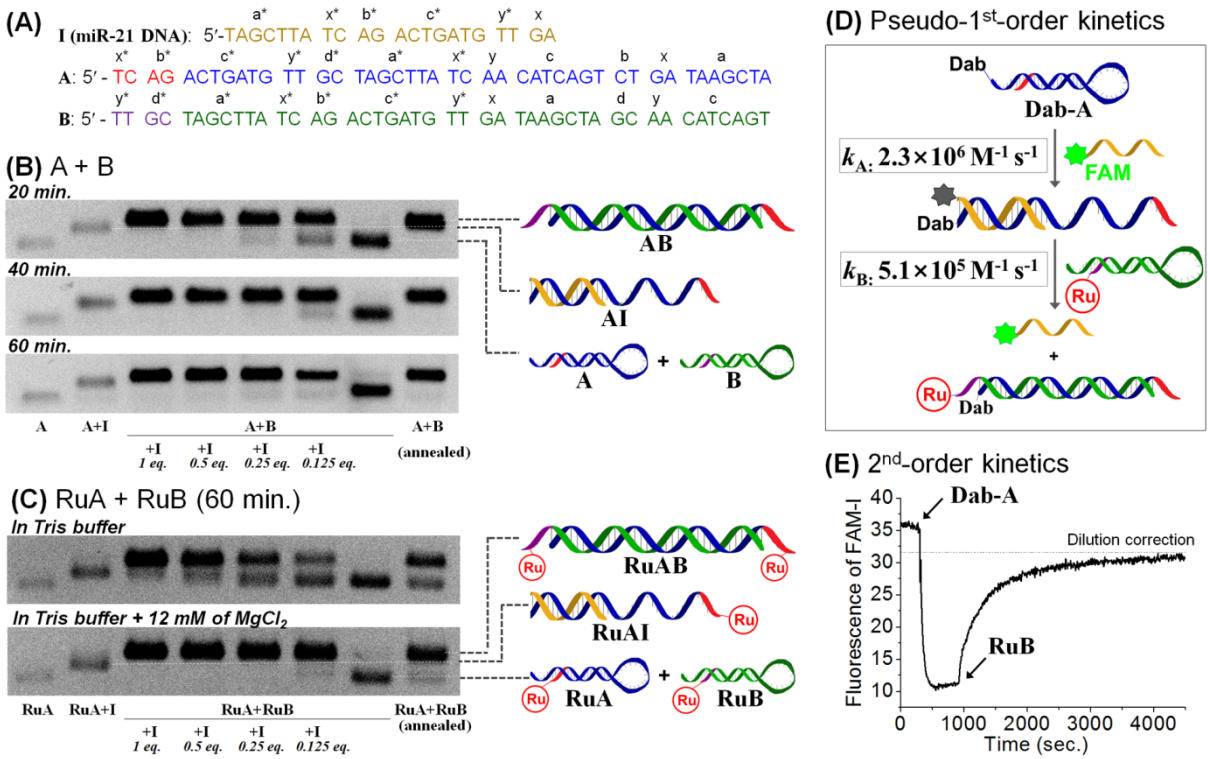

Figure 3. (A) Sequences of **A**, **B**, and **I** with segment names. **RuA** and **RuB** have exactly same sequence with **A** and **B**, respectively. DNA-fueled amplification of (B) **AB** or (C) **RuAB** duplexes bearing two sticky-ends, the sites for templated reaction, monitored by 2 % agarose gel electrophoresis. The **RuAB** circuitry is accelerated by addition of 12 mM of $MgCl_2$. (D) Fluorescence quenching experiments for determination of kinetic parameters (k_A and k_B) of DNA circuit. (E) Plot of fluorescence quenching experiments performed with stoichiometric additions of **Dab-A** to **FAM-I** followed by **RuB** (second order kinetic measurments). Every experiment was carried out in general Tris buffer conditions: 20 mM pH 7.5 Tris, 140 mM NaCl, 5 mM KCl, 12 mM $MgCl_2$, 0.02 % tween-20, 37 °C (reaction performed at 10 nM or reagents).

ruthenium had a positive impact on the rate of that step (2-fold acceleration, see Figure S4 for rate analysis), presumably due to increased ionic interactions.[34] Notably, the kinetics of the present system, featuring 7-mer toehold, is 3 to 23-times faster than that observed in prior DNA-fueled amplifier with shorter toehold (6-mer: 1.0×10^5 M^{-1} s^{-1}).[8] The overall data clearly show that the first amplification step, a toehold-fueled circuit, is successfully performed in the presence of miR-21 DNA, exhibiting fast kinetics and negligible leakage products.

The product of the DNA circuit is a duplex having two 4-mer sticky ends at 5′-ends, which serve as sites for templated reactions. While this is generally too short for DNA-templated reaction, we anticipated that the base-staking arising from hybridization at a sticky-end may offset the length deficiency. To evaluate the impact of this additional stability, we used a truncated version of the **RuA:RuB** duplex in order to study each catalytic site individually (**RuS1**:**PC** and **RuS2**:**PC**). We measured the rate of templated coumarin uncaging as a function of time. Among different types of PNA modifications tested, we found that N-acetylated serine-modified[35-36] 4-mer PNA performed best (See Figure S5 for comparison of different PNA backbones).

Gratifyingly, the templated reaction on a sticky end afforded fast conversion (Figure 4A, **P1**+**RuS1**+**PC**, $t_{1/2}$<3 min) whereas ssDNA template (absence of sticky end) showed significantly slower conversion (**P1**+**RuS1**, $t_{1/2}$~40 min). This comparison demonstrates the importance of base stacking in the templated reactions. However, in the case of **RuS2**+**P2′**+**PC** (the second sticky end site of **RuA:RuB** duplex) the reaction was found to be slower ($t_{1/2}$ ~16 min, Figure S6). This was attributed to the weaker stacking interaction of pyrimidine (C) at N-terminal of **P2′** with 3′-end of **PC** *vs* a purine in **P1**. This loss of stacking interaction was overcome with the replacement of cytosine with a phenoxazine nucleobase (Pz, Figure 4) which has an extend π-surface area and improves stacking onto the sticky end. The Pz-containing PNA (**P2**) performed comparably to **P1** in templated reaction (Figure 4B and S6 for detailed analysis). Importantly, the 4-mer reaction was highly sequence-selective (Figure S7) and the use of a full complementary sequence (**FC**) without sticky-ends afforded catalytically inactive duplexes and negligible templated reaction (Figure S8). Taken together, the data established that the templated reaction arises from duplex formation at 4-mer sticky ends and this reaction is shut down by masking the templating sequence in dsDNA.

We next measured the reactions' half-life at higher template loading (1-6 μM), measuring an apparent rate constants (k_{app}) of 0.087 s^{-1} for both reactions (Figure 4B and S9, **P1** and **P2**) at 25 °C. Notably, this rate 38-fold faster than that of PNA-PNA templated reaction with 4-mer (reaction lacking the stabilization of a sticky end).[26]

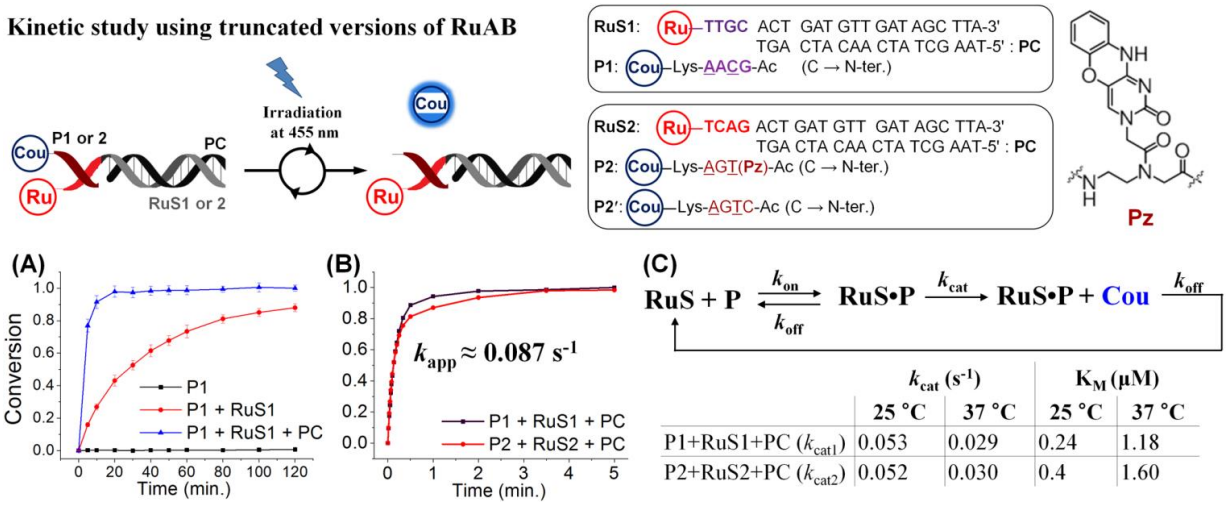

	k_{cat} (s^{-1})		K_M (μM)	
	25 °C	37 °C	25 °C	37 °C
P1+RuS1+PC (k_{cat1})	0.053	0.029	0.24	1.18
P2+RuS2+PC (k_{cat2})	0.052	0.030	0.4	1.60

Figure 4. Templated reaction on DNA sticky-ends using truncated versions of the **RuA**:**RuB** duplex. Underlined residues represent serine-modified PNA. (A) Templated reaction between **P1** and **RuS1** using 1:1 stoichiometry (50 nM) at 25 °C in the presence or absence of **PC** strand. (B) k_{app} of **P1** and **P2** with **RuS1**:**PC** and **RuS2**:**PC** respectively (6 μM, 1:1 stoichiometry). (C) Catalytic performance of **RuS** and measurments of k_{cat} and K_M from Lineweaver–Burk plot.

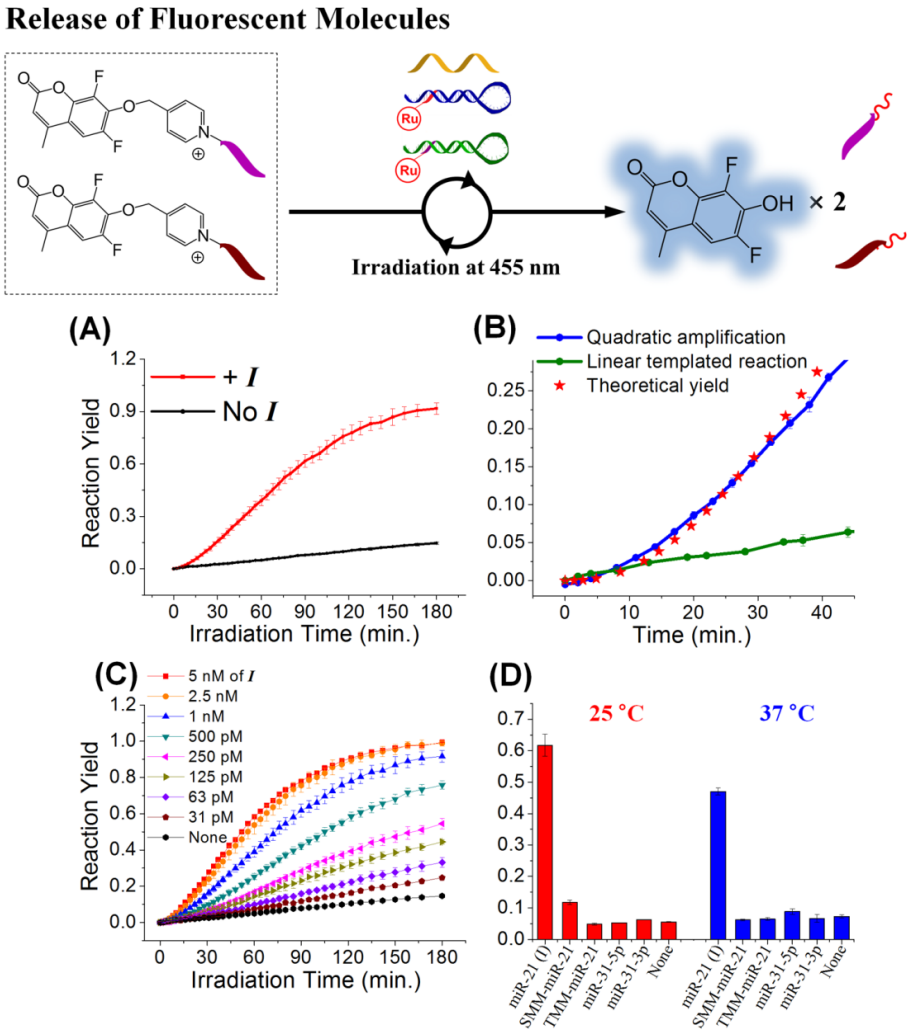

Figure 5. Quadratic behavior of templated amplification coupled with toehold-fueled amplification at 25 °C. (A) Templated reaction performed with or without 0.2 eq. of **I**. (B) Initial stage of the quadratic (5 nM of **RuA** and **RuB**) and linear templated reaction (1 nM of **RuA** and **RuB**) in the presence of 1 nM of **I**. Templated reaction yield in the presence of different (C) concentration of **I** or (D) types of oligonucleotide sequences (1 nM, 90 min of irradiation time). General conditions: 150 nM of PNAs, 5 nM of DNAs, 20 mM pH 7.5 Tris, 140 mM NaCl, 5 mM KCl , 12 mM $MgCl_2$, 0.02 % tween-20, 5 mM sodium ascorbate, 25 °C, 200 μL, data was taken right after adding **I**. miR-21, SMM-miR-21, and TMM-miR-21 are DNA sequences. miR-31-5p and 3p are RNA sequences.

To investigate the kinetics in the presence of catalytic amount of ruthenium complexes, initial rate of each reaction was monitored at increasing concentrations of **P1** or **P2** (substrate) at 25 °C. Assuming Michaelis–Menten kinetics, we determined k_{cat} and K_M based on Lineweaver–Burk plot (Figure 4C and S10): k_{cat} = 0.053 and 0.052 s^{-1} ; K_M = 0.24 and 0.4 µM for **P1** and **P2**, respectively. The reaction performed well at both 25 and 37 °C. As expected, the K_M of the templated reaction were higher at 37 °C *vs* 25 °C.

We next investigated the coupling of DNA-fueled circuit to the templated reactions. This is expected to be quadratic amplification, in which templated reactions accelerate with the accumulation of **RuA:RuB** generated by the DNA circuit. As shown in Figure 5A, a clear rate acceleration is indeed observed using 20% of initiator relatively to **RuA** and **B** (5 nM) and 30-fold excess substrates (150 nM, see also Figure S11 for reaction performed at different hairpin concentrations). Comparing this exponential amplification reaction to a linear amplification reaction with the preformed catalyst (**RuA**:**RuB**) at the same loading of the initiator, we observed that the exponential amplification surpasses the linear amplification within a few minutes (Figure 5B). Using the kinetic data measured for the individual steps of the system, we calculated the theoretical kinetics of amplification and found a good agreement with the experimental results (Figure 5B). Within 40 min, this amplification afforded > 80 nM of product from 1 nM of input. The maximum rate determined by the slope at 60 min is 6-fold faster than the linear templated reaction. This value is slightly lower than calculated by the theoretical model, however, this model does not take into consideration the competition of spent PNA reagent competing with unreacted PNA reagent for templated hybridization (product inhibition). Considering that the system has already reached >25% conversion at 60 min, some product inhibition is to be expected. Similar quadratic progressions were observed across different initiator concentrations (31 pM-5 nM of **I**, Figure 5C) and also at 37 °C (Figure S12). Notably, in case of 31 pM of **I**, the yield (30 nM) corresponded to 960-fold amplification. Increasing the PNA concentration to 5 µM further accelerated the reaction, producing a total of 3.5 µM concentration of uncaged coumarin (corrected for the background reaction) after 80 min of irradiation (Figure S13, 5 µM of **P1** and **P2**, 10 nM of **RuA** and **RuB**, 1 nM of **I**, 30 min preincubation at 37 °C). This represent a 3500-fold amplification and exceed background by 350%. Based on the DNA circuit kinetics, conversion to **RuA**:**RuB** represent > 9 turnovers of I, while each catalytic sites performed >195 turnovers in the templated reaction. The amplification also showed high selectivity for target **I** over even single mismatched (SMM) DNA or RNA sequences (Figure 5D). Taken together, the results demonstrate unprecedented amplification by the concerted action of a DNA-amplification circuit with a templated reaction.

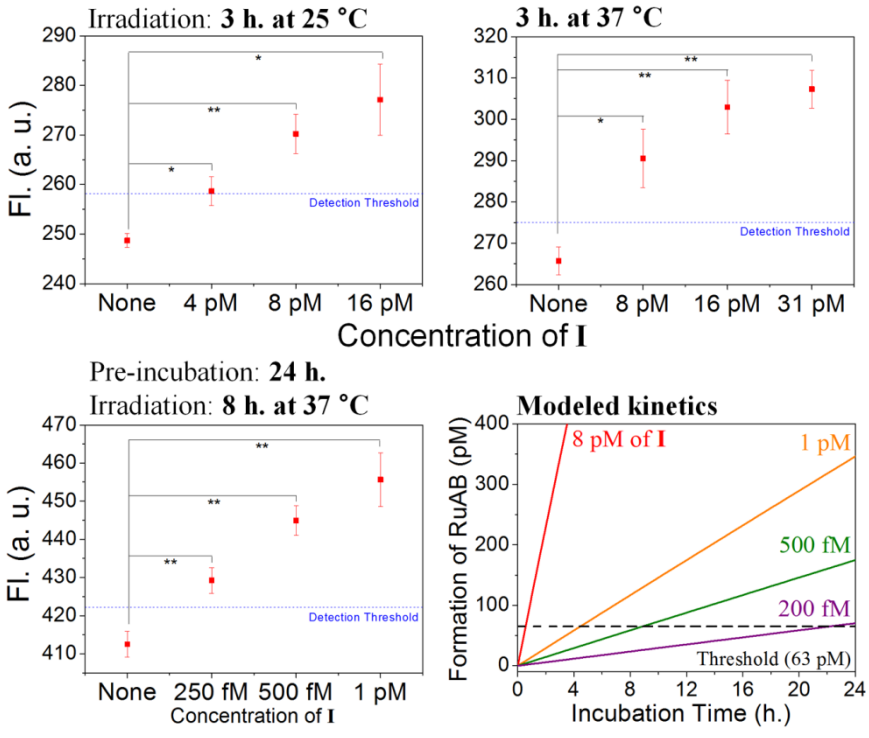

Figure 6. Detection threshold of quadratic amplification reaction tested with different irradiation and pre-incubation times. Experiments were performed in general conditions. Modeled kinetics of **RuAB** DNA circuitry indicated that >200 fM of **I** produced approximately 60 pM of **RuAB**, corresponding to the detection threshold of linear templated reaction, after 24 h of pre-incubation at 37 °C. Statistics were calculated using an unpaired two-sample t-test (*p < 0.05, **p < 0.01). Detection threshold was defined as the average of the no initiator (none) plus three times the standard deviation.

To gain insight into the detection threshold of this system, we measured endpoint fluorescence of amplification at diminishing concentration of input sequence **I**. After 3 h, discrimination of **I** *vs* control (no **I**) was possible down to 8 pM (1.6 fmol, Figure 6). Pushing the reaction to 8 h led to further gain in sensitivity with detection down to 2 pM (400 amol, Figure S14). However, the kinetic models clearly indicated that at low pM concentration, the DNA circuit is much slower than the templated reaction and the system would benefit from preincubation before irradiation. Preincubation of the reaction for 24h followed by 8h irradiation led to a significant improvement of detection in the sub-picomolar range of **I** (Figure 6, see figure S14-15 for intermediate preincubation times). This detection threshold is consistent with the kinetic model calculation that suggest that >200 fM of **I** are required to produce the minimum concentration of **RuA:RuB** (63 pM) for detection (Figure S16). This kinetic model also provides a framework to predict the reaction time necessary for a given detection threshold.

Based on properties of this quadratic amplification with a DNA circuit, this system was expected to be suitable for micromolar release of bioactive molecules using nano- or sub-nanomolar concentration of nucleic acid input. To this end, 5-fluorouracil (5-FU), an anti-cancer drug, was selected as a target of release. This drug has IC_{50} range in the high nM to low µM in the most of cell lines.[37-39] 5-FU was caged with the pyridinium linker through *O*2 position and conjugated to the PNA sequences required for templated reaction (**5FUP1 & 2**, Figure 7). To confirm release of 5-FU, the reaction was first performed at high concentration (20 µM of **5FUP2**) in order to be analyzable by HPLC. A near quantitative conversion of the caged 5-FU to 5-FU was observed based on the HPLC traces (Figure 7A). We confirmed that the pyridinium-linked PNA did mask the function of 5-FU in a cytotoxicity assay against HT-29 (colon adenocarcinoma).[40-42] As shown in Figure 7B, while 5-FU showed the expected cytotoxicity with an IC_{50} of 350 nM in HT-29 (colorectal adenocarcinoma), the caged version did not reach the measurable toxicity at 10 µM (Figure 7B).

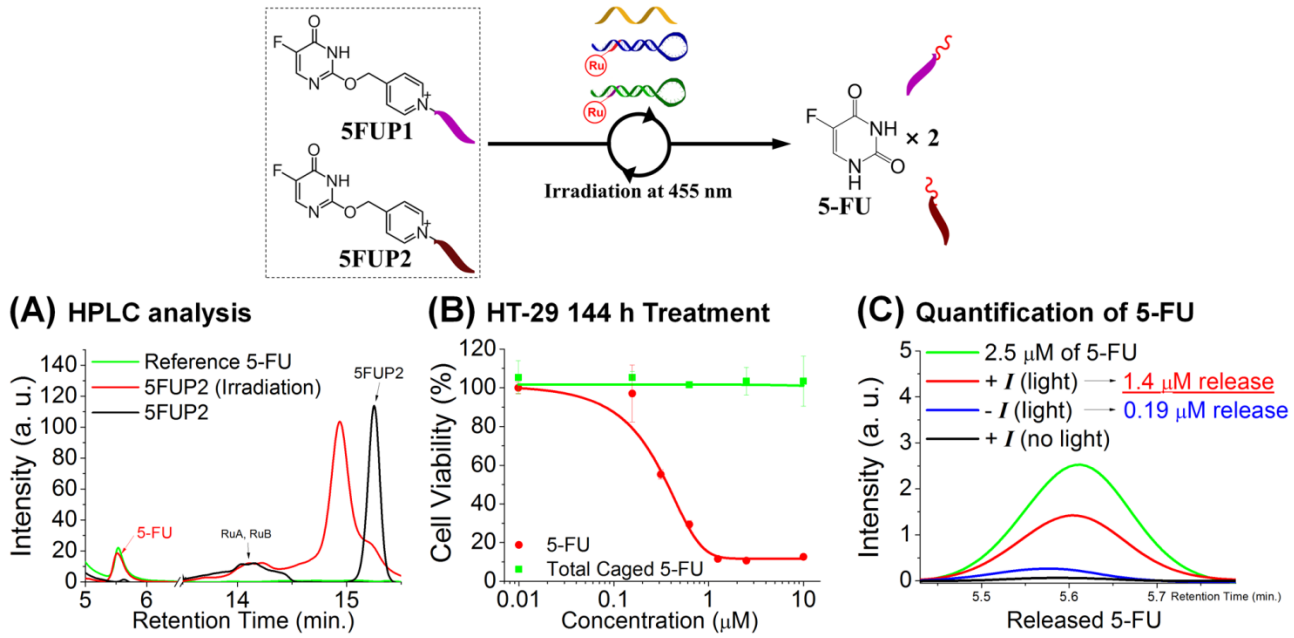

Figure 7. Release of functional molecule, 5-FU, by templated reaction coupled with DNA circuit. (A) HPLC analysis of released 5-FU from the templated reaction. Conditions: 2 h of irradiation, 20 µM of **5FUP2** , 1 µM of **RuA** and **RuB**, 100 nM of **I**, 5 mM sodium ascorbate, total V. 100 µL in general buffer. (B) Cytotoxicity assay of 5-FU and caged drugs (**5FUP1**+**5FUP2**) using HT-29 cells. (C) HPLC analysis of 5-FU released by the coupled system in the presence of 1 nM of **miR-21-5** with irradiation (light) or without irradiation (no light). The area of 0.25 µM 5-FU (0.25 nmol / 100 µL) was used as the reference. Reaction conditions before direct injection: 0.5 h of irradiation, 4 h of pre-incubation, 5 µM of each **5FUP1** and **5FUP2**, 60 nM of **RuA** and **RuB**, 1 nM of **miR-21-5**, 5 mM of sodium ascorbate, total V. 100 µL in general buffer.

We next set out to test the reaction in conditions that emulate the trigger by a circulating RNA. To this end, the reaction was performed with microRNA-21-5p, the mature bioactive form of miR-21, an abundant miR biomarker of cancer.[23] The reaction was performed at 5 µM of PNA **5FUP1** and **5FUP2** (i.e. 10 µM prodrug concentration). The uncaging was performed with 30 min irradiation following a 4 h incubation in the presence or absence of 1 nM of **miR-21-5p**. In the presence of miR-21-5p, the reaction yielded a 1.4 µM of 5-FU, a concentration significantly above the IC_{50}, while in the absence of **miR-21-5p**, the reaction resulted in a concentration inferior to a significant cytotoxicity threshold (0.19 µM. Figure 7C, see S18 for detailed quantification). In the absence of light, no measurable reaction was observed. This experiment demonstrates a >1000-fold amplification in the output of a bioactive small molecule from 1 nM input. Finally, the products of amplification reactions were added to cell culture to confirm the cytotoxicity of the uncaged product and lack of cytotoxicity of the reaction components (See Figure S19, **RuA**, **RuB**, prodrug) in the absence of light. While this is only a proof of principle and the system likely needs further optimization to be operative in live organisms, it does demonstrate that a nucleic acid input can be converted into a small molecule cytotoxic with >1000-fold amplification.

CONCLUSION

We report a system to convert a nucleic acid input to a functional small molecule output with greater than 1000-fold amplification in less than 3h under isothermal conditions. This level of amplification was enabled by the coupling of a DNA circuit and templated chemical reactions. A critical finding is that templated reactions are enhanced by sticky-end hybridization, thus extending the scope of templated reaction to very short overhang sequences (4-mer). This effect is accentuated by a purine at the position interacting with the sticky end of the template. However, nucleobase

surrogates of pyrimidine with larger π-surface area (e.g. C to Pz substitution) can be used for pyrimidines. The kinetics of all the steps in the network were characterized, thus providing a theoretical framework for the performance of the system. We demonstrated its predictive value to establish the reaction times required for a given output yield from a given input loading. We demonstrated that the amplification allowed detection of nucleic acid analytes down to 250 fM concentration and the system offered strong discrimination for even a single base pair mismatch in the input nucleic acid sequence. The system was also capable of reaching micromolar release of molecules in the presence of nanomolar or sub-nanomolar trigger signal (nucleic acid sequence). This high level of trigger amplification was used to release a cytotoxic drug (5-FU) using 1 nM of input (sequence of microRNA21-5p). While the present work made use of the microRNA-21 sequence, this design can be adapted to any nucleic acid trigger of 20-25 nt. The high sensitivity, sequence selectivity, and large amplification stem from the quadratic behavior of a DNA-amplifier circuit coupled to DNA-templated reactions. The major limitation of templated reactions is the trade-off between probe affinity and turnover frequency; longer probes having high template affinity show slow turnover kinetics. The present system reconciles this trade off by decoupling the response to templated reaction. First, the DNA circuit generates the catalyst for templated reactions with fast kinetics and turnover for long trigger sequences. Second, 4-mer sticky ends are utilized as sites for templated reaction affording one of the fastest k_{cat} (0.05 s^{-1}) amongst templated reactions.

ASSOCIATED CONTENT

The Supporting Information is available free of charge on the ACS Publications website at DOI: I: 10.1021/jacs.9b05688
Supplementary figures, experimental protocols, synthetic procedures and compound characterization. Raw data associated with experiments reported has been deposited and is available (https://zenodo.org/record/3337874#.XZHc9y2B2ys).

AUTHOR INFORMATION

Corresponding Author

*nicolas.winssinger@unige.ch.

Author Contributions

The manuscript was written through contributions of all authors. All authors have given approval to the final version of the manuscript.

Notes

The authors declare no competing financial interest.

ACKNOWLEDGMENT

The authors thank the SNSF (grant: 200020_169141) and the NCCR Chemical Biology for financial support

REFERENCES

(1) Seeman, N. C., DNA in a material world. *Nature* **2003,** *421*, 427-431.
(2) Seeman, N. C.; Sleiman, H. F., DNA nanotechnology. *Nat. Rev. Mater.* **2018,** *3*, 17068.
(3) Lehn, J. M., Toward self-organization and complex matter. *Science* **2002,** *295*, 2400-2403.
(4) Zhang, D. Y.; Winfree, E., Control of DNA Strand Displacement Kinetics Using Toehold Exchange. *J. Am. Chem. Soc.* **2009,** *131*, 17303-17314.
(5) Srinivas, N.; Ouldridge, T. E.; Sulc, P.; Schaeffer, J. M.; Yurke, B.; Louis, A. A.; Doye, J. P.; Winfree, E., On the biophysics and kinetics of toehold-mediated DNA strand displacement. *Nucleic Acids Res.* **2013,** *41*, 10641-58.
(6) Zhang, D. Y.; Seelig, G., Dynamic DNA nanotechnology using strand-displacement reactions. *Nat. Chem.* **2011,** *3*, 103-113.
(7) Zhang, D. Y.; Turberfield, A. J.; Yurke, B.; Winfree, E., Engineering entropy-driven reactions and networks catalyzed by DNA. *Science* **2007,** *318*, 1121-5.
(8) Yin, P.; Choi, H. M. T.; Calvert, C. R.; Pierce, N. A., Programming biomolecular self-assembly pathways. *Nature* **2008,** *451*, 318-324.
(9) Qian, L.; Winfree, E., Scaling up digital circuit computation with DNA strand displacement cascades. *Science* **2011,** *332*, 1196-201.
(10) Krishnan, Y.; Simmel, F. C., Nucleic acid based molecular devices. *Angew. Chem. Int. Ed. Engl.* **2011,** *50*, 3124-56.
(11) Wang, F.; Lu, C. H.; Willner, I., From cascaded catalytic nucleic acids to enzyme-DNA nanostructures: controlling reactivity, sensing, logic operations, and assembly of complex structures. *Chem. Rev.* **2014,** *114*, 2881-941.
(12) Wu, C. C.; Cansiz, S.; Zhang, L. Q.; Teng, I. T.; Qiu, L. P.; Li, J.; Liu, Y.; Zhou, C. S.; Hu, R.; Zhang, T.; Cui, C.; Cui, L.; Tan, W. H., A Nonenzymatic Hairpin DNA Cascade Reaction Provides High Signal Gain of mRNA Imaging inside Live Cells. *J. Am. Chem. Soc.* **2015,** *137*, 4900-4903.
(13) Morihiro, K.; Ankenbruck, N.; Lukasak, B.; Deiters, A., Small Molecule Release and Activation through DNA Computing. *J. Am. Chem. Soc.* **2017,** *139*, 13909-13915.
(14) Sun, X.; Wei, B.; Guo, Y.; Xiao, S.; Li, X.; Yao, D.; Yin, X.; Liu, S.; Liang, H., A Scalable "Junction Substrate" to Engineer Robust DNA Circuits. *J. Am. Chem. Soc.* **2018,** *140*, 9979-9985.
(15) Simmel, F. C.; Yurke, B.; Singh, H. R., Principles and Applications of Nucleic Acid Strand Displacement Reactions. *Chem. Rev.* **2019**, *119*, 6326-6369 .

(16) Gorska, K.; Winssinger, N., Reactions Templated by Nucleic Acids: More Ways to Translate Oligonucleotide-Based Instructions into Emerging Function. *Angew. Chem. Int. Ed. Engl.* **2013,** *52*, 6820-6843.
(17) Di Pisa, M.; Seitz, O., Nucleic Acid Templated Reactions for Chemical Biology. *ChemMedChem* **2017,** *12*, 872-882.
(18) Benenson, Y.; Gil, B.; Ben-Dor, U.; Adar, R.; Shapiro, E., An autonomous molecular computer for logical control of gene expression. *Nature* **2004,** *429*, 423-429.
(19) Rothlingshofer, M.; Gorska, K.; Winssinger, N., Nucleic Acid-Templated Energy Transfer Leading to a Photorelease Reaction and its Application to a System Displaying a Nonlinear Response. *J. Am. Chem. Soc.* **2011,** *133*, 18110-18113.
(20) Mitchell, P. S.; Parkin, R. K.; Kroh, E. M.; Fritz, B. R.; Wyman, S. K.; Pogosova-Agadjanyan, E. L.; Peterson, A.; Noteboom, J.; O'Briant, K. C.; Allen, A.; Lin, D. W.; Urban, N.; Drescher, C. W.; Knudsen, B. S.; Stirewalt, D. L.; Gentleman, R.; Vessella, R. L.; Nelson, P. S.; Martin, D. B.; Tewari, M., Circulating microRNAs as stable blood-based markers for cancer detection. *Proc. Natl. Acad. Sci. USA* **2008,** *105*, 10513-10518.
(21) Dong, H. F.; Lei, J. P.; Ding, L.; Wen, Y. Q.; Ju, H. X.; Zhang, X. J., MicroRNA: Function, Detection, and Bioanalysis. *Chem. Rev.* **2013,** *113*, 6207-6233.
(22) Fish, L.; Zhang, S.; Yu, J. X.; Culbertson, B.; Zhou, A. Y.; Goga, A.; Goodarzi, H., Cancer cells exploit an orphan RNA to drive metastatic progression. *Nat. Med.* **2018,** *24*, 1743-1751.
(23) Umu, S. U.; Langseth, H.; Bucher-Johannessen, C.; Fromm, B.; Keller, A.; Meese, E.; Lauritzen, M.; Leithaug, M.; Lyle, R.; Rounge, T. B., A comprehensive profile of circulating RNAs in human serum. *RNA Biol.* **2018,** *15*, 242-250.
(24) Chang, D. L.; Kim, K. T.; Lindberg, E.; Winssinger, N., Accelerating Turnover Frequency in Nucleic Acid Templated Reactions. *Bioconj. Chem.* **2018,** *29*, 158-163.
(25) Velema, W. A.; Kool, E. T., Fluorogenic Templated Reaction Cascades for RNA Detection. *J. Am. Chem. Soc.* **2017,** *139*, 5405-5411.
(26) Chang, D.; Lindberg, E.; Winssinger, N., Critical Analysis of Rate Constants and Turnover Frequency in Nucleic Acid-Templated Reactions: Reaching Terminal Velocity. *J. Am. Chem. Soc.* **2017,** *139*, 1444-1447.
(27) Holtzer, L.; Oleinich, I.; Anzola, M.; Lindberg, E.; Sadhu, K. K.; Gonzalez-Gaitan, M.; Winssinger, N., Nucleic Acid Templated Chemical Reaction in a Live Vertebrate. *ACS Cent. Sci.* **2016,** *2*, 394-400.
(28) Lindberg, E.; Angerani, S.; Anzola, M.; Winssinger, N., Luciferase-induced photoreductive uncaging of small-molecule effectors. *Nat. Commun.* **2018,** *9*.
(29) Anzola, M.; Winssinger, N., Turn On of a Ruthenium(II) Photocatalyst by DNA-Templated Ligation. *Chem. Eur. J.* **2019,** *25*, 334-342.
(30) Angerani, S.; Winssinger, N., Visible Light Photoredox Catalysis Using Ruthenium Complexes in Chemical Biology. *Chem. Eur. J.* **2019,** *25*, 6661-6672.
(31) Mooren, F. C.; Geada, M. M.; Singh, J.; Stoll, R.; Beil, W.; Domschke, W., Effects of extracellular Mg2+ concentration on intracellular signalling and acid secretion in rat gastric parietal cells. *Biochim. Biophys. Acta* **1997,** *1358*, 279-88.
(32) Farruggia, G.; Castiglioni, S.; Sargenti, A.; Marraccini, C.; Cazzaniga, A.; Merolle, L.; Iotti, S.; Cappadone, C.; Maier, J. A. M., Effects of supplementation with different Mg salts in cells: is there a clue? *Magnesium Res.* **2014,** *27*, 25-33.
(33) Mewes, A.; Langer, G.; de Nooijer, L. J.; Bijma, J.; Reichart, G. J., Effect of different seawater Mg(2 +) concentrations on calcification in two benthic foraminifers. *Mar. Micropaleontol.* **2014,** *113*, 56-64.
(34) Kim, W. J.; Akaike, T.; Maruyama, A., DNA strand exchange stimulated by spontaneous complex formation with cationic comb-type copolymer. *J. Am. Chem. Soc.* **2002,** *124*, 12676-12677.
(35) Dragulescu-Andrasi, A.; Rapireddy, S.; Frezza, B. M.; Gayathri, C.; Gil, R. R.; Ly, D. H., A simple gamma-backbone modification preorganizes peptide nucleic acid into a helical structure. *J. Am. Chem. Soc.* **2006,** *128*, 10258-10267.
(36) Chouikhi, D.; Ciobanu, M.; Zambaldo, C.; Duplan, V.; Barluenga, S.; Winssinger, N., Expanding the Scope of PNA-Encoded Synthesis (PES): Mtt-Protected PNA Fully Orthogonal to Fmoc Chemistry and a Broad Array of Robust Diversity-Generating Reactions. *Chem. Eur. J.* **2012,** *18*, 12698-12704.
(37) Wiebke, E. A.; Grieshop, N. A.; Loehrer, P. J.; Eckert, G. J.; Sidner, R. A., Antitumor effects of 5-fluorouracil on human colon cancer cell lines: antagonism by levamisole. *J. Surg. Res.* **2003,** *111*, 63-69.
(38) Flis, S.; Splwinski, J., Inhibitory effects of 5-fluorouracil and oxaliplatin on human colorectal cancer cell survival are synergistically enhanced by sulindac sulfide. *Anticancer Res.* **2009,** *29*, 435-441.
(39) Tong, J.; Xie, G.; He, J.; Li, J.; Pan, F.; Liang, H., Synergistic antitumor effect of dichloroacetate in combination with 5-fluorouracil in colorectal cancer. *J. Biomed. Biotechnol.* **2011,** *2011*, 740564.
(40) Violette, S.; Poulain, L.; Dussaulx, E.; Pepin, D.; Faussat, A. M.; Chambaz, J.; Lacorte, J. M.; Staedel, C.; Lesuffleur, T., Resistance of colon cancer cells to long-term 5-fluorouracil exposure is correlated to the relative level of Bcl-2 and Bcl-X(L) in addition to Bax and p53 status. *Int. J. Cancer* **2002,** *98*, 498-504.
(41) Touil, Y.; Igoudjil, W.; Corvaisier, M.; Dessein, A. F.; Vandomme, J.; Monte, D.; Stechly, L.; Skrypek, N.; Langlois, C.; Grard, G.; Millet, G.; Leteurtre, E.; Dumont, P.; Truant, S.; Pruvot, F. R.; Hebbar, M.; Fan, F.; Ellis, L. M.; Formstecher, P.; Van Seuningen, I.; Gespach, C.; Polakowska, R.; Huet, G., Colon cancer cells escape 5FU chemotherapy-induced cell death by entering stemness and quiescence associated with the c-Yes/YAP axis. *Clin. Cancer Res.* **2014,** *20*, 837-846.
(42) Leong, K. H.; Looi, C. Y.; Loong, X. M.; Cheah, F. K.; Supratman, U.; Litaudon, M.; Mustafa, M. R.; Awang, K., Cycloart-24-ene-26-ol-3-one, a New Cycloartane Isolated from Leaves of Aglaia exima Triggers Tumour Necrosis Factor-Receptor 1-Mediated Caspase-Dependent Apoptosis in Colon Cancer Cell Line. *PLoS One* **2016,** *11*, e0152652.

TOC

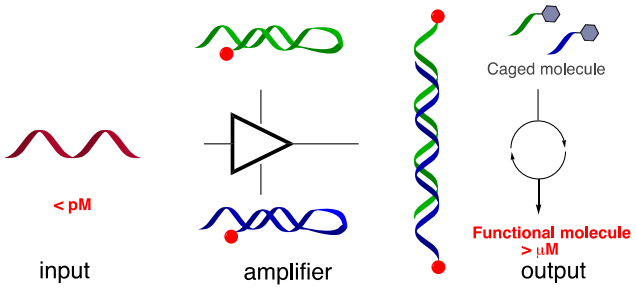
< pM
input
amplifier
Caged molecule
Functional molecule
> μM
output